Effect of the Shaft Stiffness on the Inertial Response of the Fixed Speed Wind Turbines and Its contribution to the System Inertia

GONZÁLEZ-LONGATT Francisco[1,2,*], REGULSKI Pawel[1], NOVANDA Happy[1], TERZIJA Vladimir[1]

[1] *School of Electrical Engineering, The University of Manchester, Manchester M13DD, United Kingdom;*
[2] *Vice-President of Venezuelan Wind Energy Association, Caracas 1010, Venezuela;*

Abstract: Future power system faces several challenges; one of them is the high penetration level of intermittent wind power generation, which provide small or even no inertia response, not contributing to the frequency stability. In this paper, the effect of the shaft stiffness on the inertial response of the fixed speed wind turbines and its contribution to the system inertia is presented. Four different drivetrain models based on the Multi-body System are presented in this paper. The small-signal analysis of them demonstrated no significant difference between models in terms of electro-mechanical eigen-values for increasing of shaft stiffness. The natural resonance frequency of the torsional modes of the drivetrain show slightly different values between damped and undapmped models but not significant differences are found in the number-mass model. Time-domain simulations show the changes in the active power contribution of a wind farm based on fixed speed wind turbine during system frequency disturbance. The changes in the kinetic energy during the dynamic process have been calculated and their contribution to the inertia constant has been found small but effective. The largest contribution of the kinetic energy is provided at the very beginning of the system frequency disturbance helping to reduce the Rate of Change of Frequency, which is positive for the frequency stability.

Keywords: induction generator, inertial response, sub-synchronous oscillation, wind energy, wind power, wind turbine

1 Introduction

The frequency of a power system depends on real power balance: generation-demand. In the normal operation of a power system, the frequency is regulated within strict limits by adjusting the electrical supply to meet the demand [1]. If the balance between generation and demand is not reached, the system frequency will change at a rate initially determinate by the *total system inertia* [2]. The total system inertia comprises the combined inertia of most of spinning generation and load connected to the power system.

Future power system faces several challenges; one of them is the high penetration level of intermittent generators connected over converters, having available storage components. Especially, the increasing penetration of wind power into the power system introduces new challenges in the frequency control and stability [3]. Wind generators provide small or even no inertia response, not contributing to the frequency stability. A considerable reduction of the capability to overcome system's frequency disturbances will appear due to the total system-inertia reduction [4].

The contribution to the total system inertia of one load or generator depends if the system frequency causes change in its rotational speed and, then, its *kinetic energy*. The power associated with this change in kinetic energy is fed or taken from the power system and is known as the *inertial response* [2].

The inertial response of wind-turbine generators has attracted much attention in recent years. An assessment of the inertial response of a wind turbine generator system (WTGS) employing a doubly-fed induction generator (DFIG) is presented in [5] and a comparison between the inertial response of a squirrel-cage and doubly fed induction-machine-based wind-turbine generator is shown in [2]. The concept of *synthetic* or *emulated inertia* was introduced in [6], several control concepts has been developed to enable WTGS to participate in grid frequency control [4], [7]; a summary can be found in [8].

Many efforts have been made regarding the modeling and simulation of wind turbines and their main components, especially in terms of controllers. The mechanical system of the wind turbines has been studied in several publications, in specific, the drivetrain and its performance has been evaluated during short circuits [9] and transient stability [10]. However, the potential contribution of the drive train to the inertial response is one aspect not well documented.

Oscillations in *squirrel-cage induction generator* (SCIG) that are used in *fixed speed wind turbines* (FSWT) are intrinsically damped and during a system frequency disturbance the flexibility of the mechanical drive train can influence the inertial response of the FSWT.

This paper establishes the effect of the shaft stiffness on the inertial response of the FSWT. The WTGS considered in this paper comprises a FSWT that is connected to a SCIG

*Corresponding author (email: fglongatt@ieee.org)

978-1-4244-9621-1/11/$26.00 ©2011 IEEE

trough a gearbox with flexible shaft. Section 2 provides a general overview of the different drivetrain configurations used in horizontal-axis WTGS and the mathematical model for the drivetrain examined in this paper is presented. Results of the small-signal and time domain simulations are presented in Section 3. Finally, a discussion about the effect of the shaft stiffness is presented.

2 Wind Turbine Drivetrain

The term "mechanical drivetrain" encompasses all rotating parts, from the rotor hub to the electrical generator [11]. It has the important task of transforming the rotational energy of the rotor into electrical power.

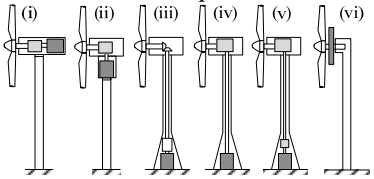

(a) Basic drive train configurations in a wind turbine: (i) Gearbox and generator in the nacelle –standard, (ii) Generator vertical in the towerhead, (iii) Gearbox in the towerfoot, (iv) Gearbox in the nacelle, generator in the towerfoot, (v) Generator in the towerfoot, two separate gearboxes, (vi) generator directly driven by the rotor (without gearbox).

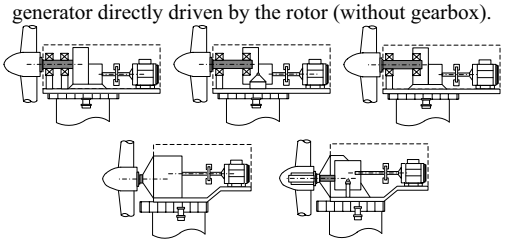

(b) Typical wind turbine rotor-shaft bearing assemblies.

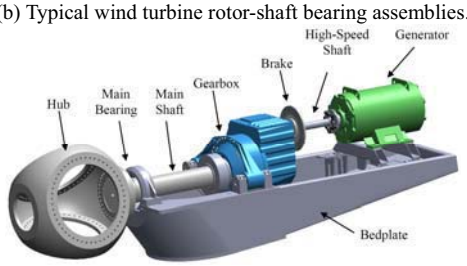

(c) Drivetrain configuration of FSWT.

Figure 1 Wind Turbine drivetrain

The drivetrain is composed of several elements, each of which contributes to a specific task. Except for the direct drivetrain, all drivetrains have a gearbox. The gearbox is a mechanical device capable of transferring torque loads from a primary mover to a rotary output, typically with a different relation of angular velocity and torque.

Horizontal axis drivetrain is composed of the following components: hub, main bearing, main shaft, gearbox, brake, generator shaft, and generator. These components form a functional unit and should, therefore, always be considered together. There are several possibilities for the drive train configurations and they are shown in Figure 1(a), however most manufacturers rely on the conventional drivetrain design with a gearbox between the rotor and the generator installed in the nacelle. There are several configurations for the assembly of the rotor-shaft bearing, Figure 1(b), however the most often used configuration in FSWT is presented in Figure 1(c). Two spherical roller bearings are used for shaft support and the gearbox is supported on the rotor shaft.

2.1 Models of Drive-train System

The drivetrain of wind turbines is composed by: soft shafts, elastic couplings, and rigid elements with inertia such as generator. For this reason, the model of the drivetrain can be derived using the so-called Multi-body System (MBS) approach. This multi-mass equivalent model provides a suitable representation for the low frequency torsional modes, which dominate the behavior of the WTGS. The following four types of drivetrain models of the WTGS are usually available in the power system analysis [12]: (a) 6-mass drive train model, (b) 3-mass drive train model, (c) 2-mass shaft model and (d) Single-mass or lumped model.

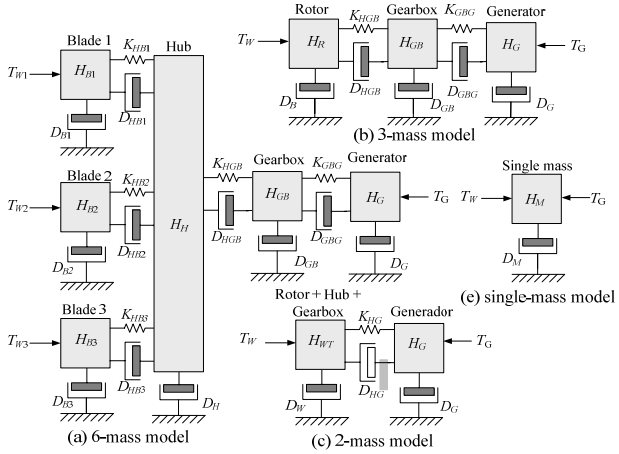

Figure 2 Schematic diagram of the traditional two-mass and one-mass equivalent model of a wind turbine [13].

(a) 6-mass model: The basic 6-mass drive train model (for a 3-blade rotor) is presented in Figure 2(a). The system model has six inertias: three blade inertias (H_{B1}, H_{B2}, and H_{B3}), hub inertia, H_H, gearbox inertia, H_{GB}, and generator inertia, H_G. θ_{B1}, θ_{B2}, θ_{B3}, θ_H, θ_{GB}, and θ_G represent angular positions of the blades, hub, gearbox and generator. ω_{B1}, ω_{B2}, ω_{B3}, ω_H, ω_{GB}, and ω_{G} correspond to the angular velocities of the blades, hub, gearbox, and generator. The state equations for the drivetrain mechanical equivalent of Figure 2(a) are the following, using the angular positions $\boldsymbol{\theta}$ and velocities $\boldsymbol{\omega}$ as state variables:

$$\begin{bmatrix}\dot{\boldsymbol{\theta}}\\ \dot{\boldsymbol{\omega}}\end{bmatrix}=\begin{bmatrix}\mathbf{0}_{6\times6} & \mathbf{I}_{6\times6}\\ -2\mathbf{H}^{-1}\mathbf{K} & -2\mathbf{H}^{-1}\mathbf{D}\end{bmatrix}\begin{bmatrix}\boldsymbol{\theta}\\ \boldsymbol{\omega}\end{bmatrix}+\begin{bmatrix}\mathbf{0}_{6\times6}\\ 2\mathbf{H}^{-1}\end{bmatrix}\mathbf{T} \qquad (1)$$

where:

$\boldsymbol{\theta}=[\theta_{B1},\theta_{B2},\theta_{B3},\theta_H,\theta_{GB},\theta_G]^T$ the vector of angular velocities of the blades, hub, gearbox and generator.

$\boldsymbol{\omega}=[\omega_{B1},\omega_{B2},\omega_{B3},\omega_H,\omega_{GB},\omega_G]^T$ the vector of angular positions.

$\mathbf{T}=[T_{B1},T_{B2},T_{B3},0,0,T_G]^T$ the vector of external torques acting.

Definitions of **H** inertia matrix, **K** stiffness matrix and **D** damping matrix are given in the Appendix.

(b) 3-mass model: Six-mass model is hardly applicable to most power systems because the model is too complicated (e.g., each blade of the wind turbine is expressed by one mass) [14]. Model depicted in Figure 2(b) consists of three lumped inertias elastically coupled to each other: rotor turbine, shaft and generator. The state equations of the 3-mass mechanical equivalent of Figure 3(b) are the following:

$$\begin{bmatrix}\dot{\boldsymbol{\theta}}\\ \dot{\boldsymbol{\omega}}\end{bmatrix}=\begin{bmatrix}\mathbf{0}_{3\times3} & \mathbf{I}_{3\times3}\\ -2\mathbf{H}^{-1}\mathbf{K} & -2\mathbf{H}^{-1}\mathbf{D}\end{bmatrix}\begin{bmatrix}\boldsymbol{\theta}\\ \boldsymbol{\omega}\end{bmatrix}+\begin{bmatrix}\mathbf{0}_{3\times3}\\ 2\mathbf{H}^{-1}\end{bmatrix}\mathbf{T} \quad (2)$$

where

$\boldsymbol{\theta}=[\theta_R,\theta_{GB},\theta_G]^T$ the vector of angular velocities of the rotor, gearbox and generator.

$\boldsymbol{\omega}=[\omega_R,\omega_{GB},\omega_G]^T$ the vector of angular positions.

$\mathbf{T}=[T_W,0,T_G]^T$ the vector of external torques acting.

Definitions of **H** inertia matrix, **K** stiffness matrix and **D** damping matrix are given in the Appendix.

(c) 2-Mass Drive Train Model: The 3-mass system can be converted into a 2-mass system, which is shown in Fig. 2(c). The drivetrain of WTs is transformed to a simple model consisting of two masses, where one lumped mass accounts for the low speed shaft (which includes the blades and hub), and the other one accounts for the high-speed shaft (which includes the rotor of the generator). The state model of motion for this two-mass model is given:

$$\begin{bmatrix}\dot{\theta}_B\\ \dot{\omega}_W\\ \dot{\omega}_G\end{bmatrix}=\begin{bmatrix}0 & 1 & -1\\ -\frac{K_{HG}}{2H_W} & -\frac{D_{HG}+D_W}{2H_W} & +\frac{D_{HG}}{2H_W}\\ \frac{K_{HG}}{2H_W} & \frac{K_{HG}}{2H_W} & -\frac{D_{HG}+D_G}{2H_W}\end{bmatrix}\begin{bmatrix}\theta_B\\ \omega_W\\ \omega_G\end{bmatrix}+\begin{bmatrix}0 & 0\\ \frac{1}{2H_W} & 0\\ 0 & \frac{1}{2H_G}\end{bmatrix}\begin{bmatrix}T_W\\ T_G\end{bmatrix} \quad (4)$$

where $H_{WT} = H_b + H_H + H_{GB}$ is the wind turbine inertia constant (which includes the blades and hub).

(d) One-mass lumped model: One lumped mass accounts for all the rotating components of the wind turbine drive train. The differential equations of motion for this two-mass model are given:

$$2H_M\frac{d\omega_M}{dt}=T_W-T_G-D_M\omega_M \quad (3)$$

where $H_M = H_{WT} + H_G$ is the inertia constant of the single rotating mass (which includes the blades, hub, gearbox and generator rotor), and D_M is damping coefficient of this single mass, respectively.

2.2 Considerations about the Drive-train Sys-

The gearbox multiplies the entering speed to obtain a usable one that goes into the generator, therefore the inertias, damping and spring constant must be corrected and be referred to one speed of rotation. The per unit (p.u.) system can be extended to the rotating mechanical system and a complete discussion of the use of p.u. system on WTGS can be found in [15]. Table 1 shows the typical values of the drivetrain data representative for wind turbines in the range from below 1MW up to 4 or 5 MW. It should be noticed that range of typical values is quite wide. However, the data of active-stall-controlled wind turbines are at the upper end of the range, whereas those for pitch-controlled WT are at the lower end of the range.

Table 1 Typical drive train data in per unit

Quantity	Typical Range
Generator rotor inertia constant, H_G (s)	0.40 – 0.80
Wind turbine inertia constant, H_W (s)	2.00-6.00
High-speed shaft stiffness, $K_{High\text{-}Shaft}$ (p.u.)	2.00-4.00
Low-speed shaft stiffness, $K_{Low\text{-}Shaft}$ (p.u.)	0.35-0.70
Total shaft stiffness, K_{HG} (p.u)	0.30-0.60

The drivetrain of a FSWT use two shafts, low and high speed, however only the low-speed shaft is incorporated to the drivetrain representation [16]. It is because FSWT has a relatively soft coupling between the generator and the SCIG [17]. On the other hand, the high-speed shaft and gearbox are considered infinitely stiff [15]. Considering typical measure of shaft stiffness, the shaft stiffness of FSWT is between 30 and 100 times lower that the stiffness found in conventional power plants units [17]. WTGS low-speed shaft is typically built from forged allow steel: 42CrMo4, 34CrNiMo6, 42CrMo, 34CrNiMo8.

3. Simulations and Results

(a) Small-Signal Analysis: The locus of the mechanical eigen-values of drivetrain with shaft stiffness increases is plotted in Figure 3, different number of mass in model is considered.

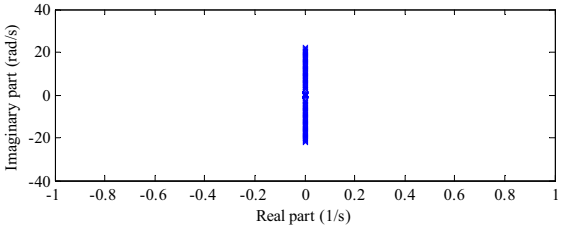

(a) 2-mass model

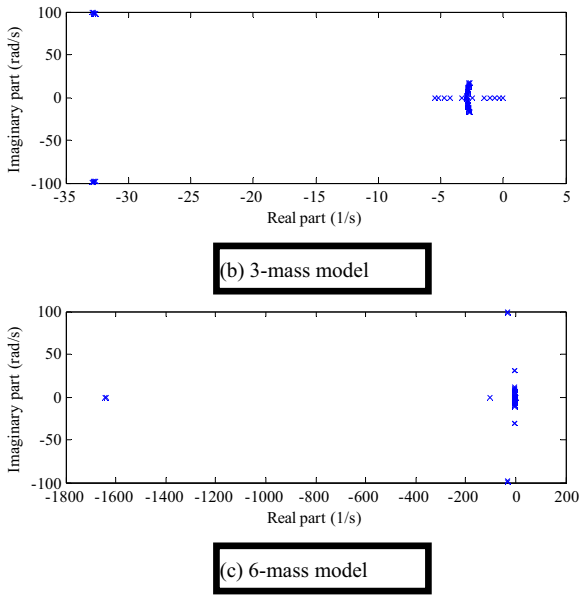

Figure 3 Electromechanical eigen-values of drivetrain for increasing of shaft stiffness.

The increase of number of masses considered in the equivalent model of the drivetrain increase the number of mechanical eigen-values.

Increases of the shaft stiffness increase the imaginary part of the mechanical eigen-values, which produces changes in the frequency of the torsional oscillations of the drivetrain, and it is shown in Figure 4. These changes are true independently of the number of masses included in the model.

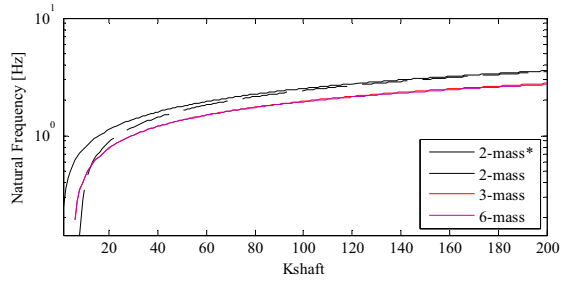

Figure 4 Natural resonance frequency (f_n) of the torsional model of the drive train for increasing of shaft stiffness. (*) Undamped model

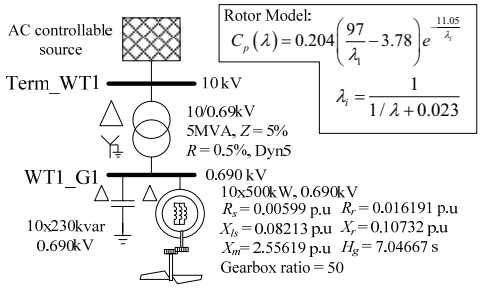

Figure 5 Test system: Wind farm 10x500 kW.

A wind farm based on 5x500 kW FSWT, as shown in Figure 5, is used to evaluate the impact on the electro-mechanical modes as consequence of changes in the shaft stiffness. The drivetrain is modeled using 2-mass equivalent model without damping, the test system is simulated using DigSILENT® PowerFactoy™ and data is processed using MATLAB®. Figure 6 illustrates the changes of the system eigen-values for increasing of shaft stiffness (K_{HGB}). When the shaft stiffness is gradually increased the damping of the electromechanical eigen-value increase considerably. The changes in the damped frequency go from 0.1414Hz to 0.7540 Hz when the K_{HGB} varies from 5 to 100×10^6 N.m.rad^{-1}, this is depicted in Figure 7. It should be noticed that the K_{HGB} increases as a consequence of increases of the damping ratio.

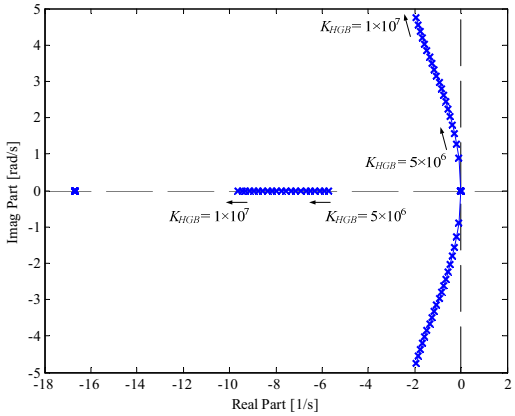

Figure 6 Electromechanical eigen-values for increasing the K_{HGB} in N.m.rad^{-1}

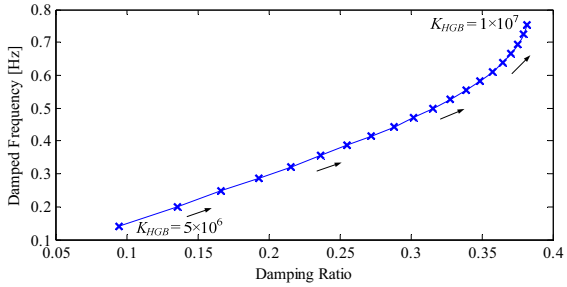

Figure 7 Impact of the increasing K_{HGB} in N.m.rad^{-1} on the electromechanical oscillations.

(b) Time-Domain simulations and Inertial Response: Time-domain simulations allow a further assessment for the effect of the inertial response of the FSWT considering the impact of the shaft to frequency disturbance. Figure 8 shows the typical inertial response of the SGIG directly connected to the grid. In this paper, the inertial response is evaluated calculating the total change in the kinetic energy (E_c) of the FSWT during a system frequency disturbance (the sum of all shadowed areas marked on Figure 8).

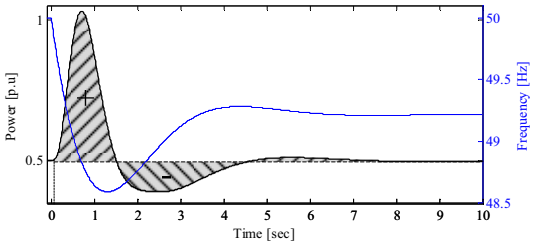

Figure 8 Typical Inertial response of a FSWT.

Figure 9 shows the inertial response of the FSWT for several values of shaft stiffness considering a step frequency decrease. Increase of damping and decrease of the oscillation frequency are consequences of increases of the shaft stiffness, which is evident on the output power of the FSWT during system frequency disturbances.

There is a relationship between the amplitude of the system frequency disturbance and the amplitude of the oscillation in the inertial response. Larges exclusions on output power oscillations are consequences of the larger frequency drop and this effect is directly related to higher values of K_{HGB}.

Energy contribution of the FSWT during the frequency disturbance is shown in Figure 10. Small shaft stiffness provide less energy that larger values and it is boosted by the size of the system frequency change.

The inertia constant (H) is defined as the ratio of kinetic energy at rated speed (E_{co}) to the rated apparent power of the machine (P_n). However, this concept is explored in this paper as changes in the inertia constant (ΔH) during the system frequency disturbance.

Using the kinetic energy contribution (E_c) plotted in Figure 10, the changes in the inertia constant have been calculated. Results show the incremental inertia is higher for high frequency changes. ΔH varies between 0.038s to 0.2 s. It represents contributions between 1.7% to 10.37%.

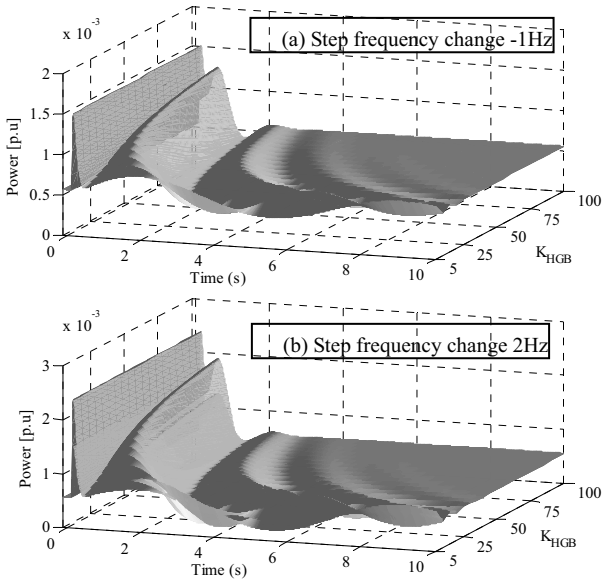

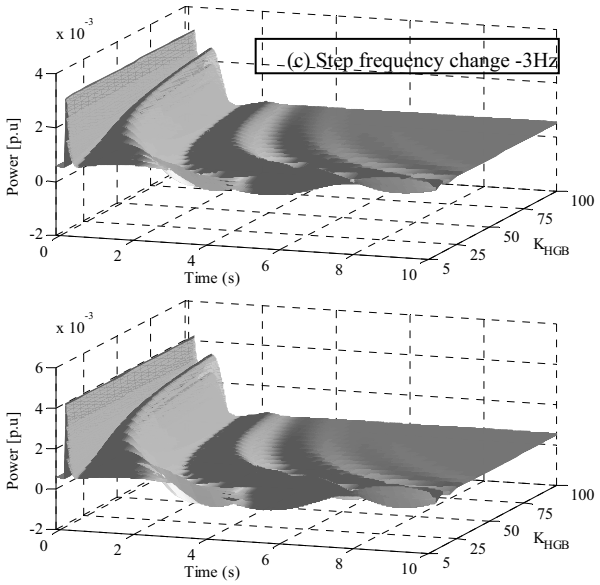

Figure 9 Inertial response of FSWT versus different K_{HGB} in $\times 10^6$ N.m.rad^{-1}.

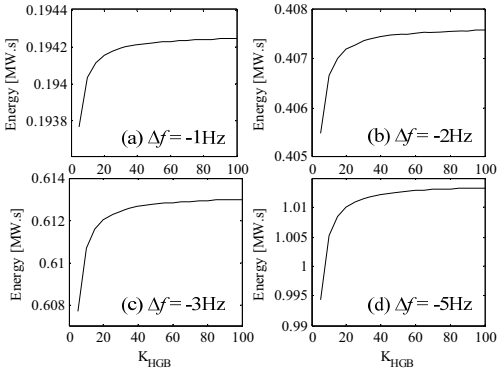

Figure 10 Energy contribution of FSWT during a frequency disturbance for several K_{HGB} values.

4 Conclusion

In this paper, the effect of the shaft stiffness on the inertial response of the FSWT and its contribution to the system inertia is presented. The model of the drivetrain is formulated based on the so-called Multi-body System (MBS) approach. Four types of drivetrain models are given in this paper. The small-signal analysis of the models demonstrated no indicative difference between models when the electro-mechanical eigen-values for increasing of shaft stiffness is plotted. The natural resonance frequency of the torsional modes of the drive train show slightly different values between damped and un-damped models for increasing of shaft stiffness demonstrated but no significant difference is found between number-mass models. Time-domain simulations show the changes in the active power contribution of the FSTW during system frequency disturbance and the energy during the dynamic process has been calculated.

Using an approach of changes in the kinetic energy the contribution to the inertia constant has been calculated. The inertia contribution depends on the magnitude of the frequency disturbance.

Appendix

$\mathbf{0}_{n\times n}$ and $\mathbf{I}_{n\times n}$ are the zero and identity n×n matrices respectively.

(A) Six-mass model: $\mathbf{H} = diag\left(H_R, H_{GB}, H_G\right)$

$$\mathbf{K} = \begin{bmatrix} K_{HGB} & -K_{HGB} & 0 \\ -K_{HGB} & K_{HGB}+K_{GBG} & -K_{GBG} \\ 0 & -K_{GBG} & K_{GBG} \end{bmatrix}$$

$$\mathbf{D} = \begin{bmatrix} D_R + D_{HGB} & -D_{HGB} & 0 \\ -D_{HGB} & D_{GB} + D_{HGB} + D_{GBG} & -D_{GBG} \\ 0 & -D_{GBG} & D_G + D_{GBG} \end{bmatrix}$$

(B) Three-mass model:

$$\mathbf{H} = diag\left(H_{B1}, H_{B2}, H_{B3}, H_H, H_{GB}, H_G\right)$$

$$\mathbf{K} = \begin{bmatrix} K_{HB1} & 0 & 0 & -K_{HB1} & 0 & 0 \\ 0 & K_{HB2} & 0 & -K_{HB2} & 0 & 0 \\ 0 & 0 & K_{HB3} & -K_{HB3} & 0 & 0 \\ -K_{HB1} & -K_{HB2} & -K_{HB3} & K_{HB1}+K_{HB2}+K_{HB2}+K_{HGB} & K_{HGB} & 0 \\ 0 & 0 & 0 & -K_{HGB} & K_{HGB}+K_{GBG} & -K_{GBG} \\ 0 & 0 & 0 & 0 & -K_{GBG} & K_{GBG} \end{bmatrix}$$

$$\mathbf{D} = \begin{bmatrix} D_{B1}+D_{HB1} & 0 & 0 & -D_{HB1} & 0 & 0 \\ 0 & D_{B2}+D_{HB2} & 0 & -D_{HB2} & 0 & 0 \\ 0 & 0 & D_{B3}+D_{HB3} & -D_{HB3} & 0 & 0 \\ -D_{HB1} & -D_{HB2} & -D_{HB3} & D_H + D_{HGB} + D_{HB1} + D_{HB2} + D_{HB3} & -D_{HGB} & 0 \\ 0 & 0 & 0 & -D_{HGB} & D_{GB}+D_{HGB}+D_{GBG} & -D_{GBG} \\ 0 & 0 & 0 & 0 & -D_{GBG} & D_G + D_{GBG} \end{bmatrix}$$

(c) Data of the multi-mass model

Quantity	6-mass	3-mass	2-mass
H_B	0.6388	-	
H_H	0.0114	-	
H_{WT}	-	1.9277	1.9277
H_{GB}	0.0806	0.0806	
H_G	0.1419	0.1419	0.2225
K_{HB}	1259.8	-	
H_{HGB}	54.75	54.75	53.16
K_{GBG}	1834.1	1834.1	
D_B	0.004	-	
D_H	0.01	-	
D_{WT}	-	0.022	0.022
D_{GB}	0.022	0.022	
D_G	0.01	0.01	0.035
D_{HB}	12.0	-	
D_{HGB}	3.5	3.5	-
D_{GBG}	10.0	10.0	

1 H. Bevrani, Robust power system frequency control: robust tech- 1st ed. New York: Springer, 2009.

2 A. Mullane and M. O'Malley, "The Inertial Response of Induction-Machine-Based Wind Turbines," Power Systems, IEEE Transactions on, vol. 20, pp. 1496-1503, 2005.

3 B. H. Chowdhury and H. T. Ma, "Frequency regulation with wind power plants," in Power and Energy Society General Meeting - Conversion and Delivery of Electrical Energy in the 21st Century, 2008 IEEE, 2008, pp. 1-5.

4 I. Erlich and M. Wilch, "Primary frequency control by wind turbines," in Power and Energy Society General Meeting, 2010 IEEE, 2010, pp. 1-8.

5 L. Holdsworth, J. B. Ekanayake, and N. Jenkins, "Power system frequency response from fixed speed and doubly fed induction generator-based wind turbines," Wind Energy, vol. 7, pp. 21-35, 2004.

6 M. C. Jackson, S. D. Umans, R. D. Dunlop, S. H. Horowitz, and A. C. Parikh, "Turbine-Generator Shaft Torques and Fatigue: Part I - Simulation Methods and Fatigue Analysis," Power Apparatus and Systems, IEEE Transactions on, vol. PAS-98, pp. 2299-2307, 1979.

7 G. Lalor, A. Mullane, and M. O'Malley, "Frequency control and wind turbine technologies," Power Systems, IEEE Transactions on, vol. 20, pp. 1905-1913, 2005.

8 S. Yuan-zhang, Z. Zhao-sui, L. Guo-jie, and L. Jin, "Review on frequency control of power systems with wind power penetration," in Power System Technology (POWERCON), 2010 International Conference on, 2010, pp. 1-8.

9 X. Yao, L. Liang, and Z. Xing, "Dynamic Characteristic of the Drive Train of DFIG Wind Turbines during Grid Faults," in Intelligent Computation Technology and Automation, 2009. ICICTA '09. Second International Conference on, 2009, pp. 503-506.

10 S. M. Muyeen, M. H. Ali, R. Takahashi, T. Murata, J. Tamura, Y. Tomaki, A. Sakahara, and E. Sasano, "Comparative study on transient stability analysis of wind turbine generator system using different drive train models," Renewable Power Generation, IET, vol. 1, pp. 131-141, 2007.

11 E. Hau, Windturbines: fundamentals, technologies, application and economics. Berlin ; London: Springer, 2000.

12 H. Li and Z. Chen, "Transient Stability Analysis of Wind Turbines with Induction Generators Considering Blades and Shaft Flexibility," in Industrial Electronics Society, 2007. IECON 2007. 33rd Annual Conference of the IEEE, 2007, pp. 1604-1609.

13 S. M. Muyeen, J. Tamura, and T. Murata, Stability Augmentation of a Grid-connected Wind Farm, Second ed.: Springer, 2009.

14 Y. Shima, R. Takahashi, T. Murata, J. Tamura, Y. Tomaki, S. Tominaga, and A. Sakahara, "Transient stability simulation of wind generator expressed by two-mass model," Electrical Engineering in Japan, vol. 162, pp. 27-37, 2008.

15 T. Ackermann, Wind power in power systems. Chichester: John Wiley & Sons, 2005.

16 V. Akhmatov, H. Knudsen, and A. H. Nielsen, "Advanced simulation of windmills in the electric power supply," International Journal of Electrical Power & Energy Systems, vol. 22, pp. 421-434, 2000.

17 E. N. Hinrichsen and P. J. Nolan, "Dynamics and Stability of Wind Turbine Generators," Power Engineering Review, IEEE, vol. PER-2, pp. 38-39, 1982.